5-7-2018

# The Role of Torsional Dynamics on Hole and Exciton Stabilization in π-Stacked Assemblies: Design of Rigid Torsionomers of a Cofacial Bifluorene

Denan Wang
*Marquette University*, denan.wang@marquette.edu

Maxim Vadimovich Ivanov
*Marquette University*

Damian Kokkin
*Marquette University*

John Loman
*Marquette University*

Jin-Zhe Cai
*Marquette University*

***See next page for additional authors***

Accepted version. *Angewandte Chemie International Edition*, Vol. 57, No. 27 (May 7, 2018): 8189-8193. DOI. 

*Angewandte Chemie International Edition*, Vol. 57, No. 27 (May 7, 2018): 8189-8193. DOI. 

# The Role of Torsional Dynamics on Hole and Exciton Stabilization in π-Stacked Assemblies: Design of Rigid Torsionomers of a Cofacial Bifluorene

Denan Wang
Department of Chemistry, Marquette University, Milwaukee, WI
Maxim V. Ivanov
Department of Chemistry, Marquette University, Milwaukee, WI
Damian Kokkin
Department of Chemistry, Marquette University, Milwaukee, WI
John Loman
Department of Chemistry, Marquette University, Milwaukee, WI
Jin-Zhe Cai
Department of Chemistry, Marquette University, Milwaukee, WI

Scott A. Reid
Department of Chemistry, Marquette University, Milwaukee, WI
Rajendra Rathore
Department of Chemistry, Marquette University, Milwaukee, WI

## Abstract

Exciton and charge delocalization across π-stacked assemblies is of importance in biological systems and functional polymeric materials. To examine the requirements for exciton and hole stabilization, cofacial bifluorene (**F**2) torsionomers were designed, synthesized, and characterized: unhindered (model) $^{Me}$**F**2, sterically hindered $^{tBu}$**F**2, and cyclophane-like $^{C}$**F**2, where fluorenes are locked in a perfect sandwich orientation via two methylene linkers. This set of bichromophores with varied torsional rigidity and orbital overlap shows that exciton stabilization requires a perfect sandwich-like arrangement, as seen by strong excimeric-like emission only in $^{C}$**F**2 and $^{Me}$**F**2. In contrast, hole delocalization is less geometrically restrictive and occurs even in sterically hindered $^{tBu}$**F**2, as judged by 160 mV hole stabilization and a near-IR band in the spectrum of its cation radical. These findings underscore the diverse requirements for charge and energy delocalization across π-stacked assemblies.

Charge and energy dynamics across π-stacked assemblies is of critical importance in biological systems as well in the performance of functional materials.[1-3] Various π-stacked dimers capable of excimer formation and charge-resonance stabilization based upon benzene,[4-8] fluorene,[9-12] pyrene,[13, 14] and other aromatic donors[15-18] have served as model systems to gain fundamental insight into key factors controlling charge/energy stabilization. These studies have established that the extent of the cationic charge (that is, hole) and exciton stabilization/delocalization is dependent on the orbital overlap between the chromophores, and is optimal when the π-stacked assembly adopts a perfect sandwich-like arrangement, where orbital overlap and electronic coupling are at their maxima.[10, 11]

Building upon this work, recent studies comparing a model covalently linked fluorene dimer **F**2 with the van der Waals dimer of fluorene, $(\mathbf{F})_2$, have shown that the geometrical requirements for hole and exciton stabilization are distinct.[10, 11] In particular, while their ionization potentials (IPs) are identical, excimeric emission at the sandwich-like geometries is shifted to longer wavelength in **F**2 as compared to $(\mathbf{F})_2$. Thus, a slight displacement from the ideal overlap leads to a less stabilized excimer in $(\mathbf{F})_2$, while cation radical stabilization remains unchanged. In the same context, in covalently linked polyfluorenes (**F***n*, *n*=2–7) the cationic charge is delocalized over multiple fluorenes,[19, 20] while exciton delocalization is limited to two fluorenes.[21]

Importantly, the dynamics of hole and exciton transfer in **F***n* is modulated by a low-frequency torsional mode between adjacent units, as evidenced in the broad and largely unresolved band in the gas-phase excitation spectrum of **F**2.[10] Indeed, calculations show that the activation barrier for interconversion between two mirror images displaced conformers of **F**2 is only 3 kcal mol$^{-1}$, yet the electronic coupling along the interconversion coordinate varies between 0.0–0.3 eV (Figure **1** A).

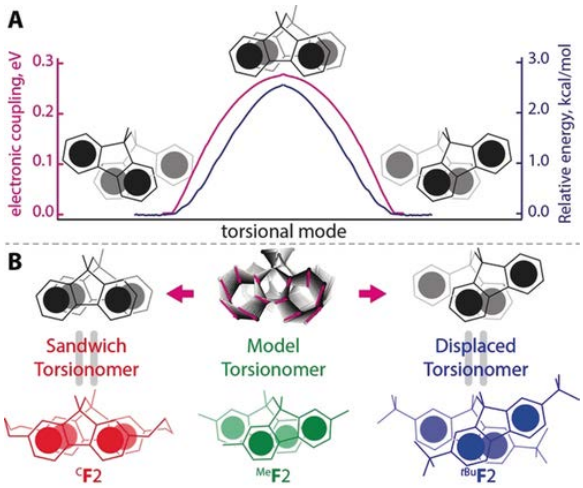


**Figure 1** A) The electronic coupling and relative energy of **F**2 calculated using B1LYP40-D3/6-31G(d)+PCM($CH_2Cl_2$) along the intrinsic reaction coordinate connecting two displaced conformations. The structure with the maximal coupling and energy is a transition state with the imaginary frequency (*i* 12.1 $cm^{-1}$) corresponding to the torsional motion. B) Representation of the torsional mode in **F**2. Incorporation of a methylene linker ($^{C}$**F**2) and substituents ($^{Me}$**F**2 and $^{tBu}$**F**2) produces various torsionomers of **F**2.

To probe the effect of cofaciality on the hole and exciton stabilization in π-stacked systems, we synthesized three rigid torsionomers of **F**2, that is, cofacial bifluorenes that differ by the extent of their cofaciality along the torsional coordinate via methylene linkers or substituents (Figure 1 B). In a cyclophane-like bifluorene $^{C}$**F**2, a pair of four-methylene linkers ensures that the relative arrangement of fluorenes is nearly identical to that found in the excimer and dimer cation radical of unsubstituted **F**2. In contrast, bulky *t*Bu groups in $^{tBu}$**F**2 guarantee that the sandwich-like arrangement is highly energetically unfavorable owing to increased steric hindrance. We then compare the redox and optoelectronic properties of the two torsionomers with those of model monomeric $^{Me}$**F**1/$^{tBu}$**F**1 and model bichromophoric $^{Me}$**F**2, the geometrical properties of which are nearly identical to those of unsubstituted **F**2.

The bifluorene $^{R}$**F**2**H**2 precursor was generated by the condensation reaction between readily available[22, 23] $^{R}$**F** and 0.5 equivalent of paraformaldehyde with potassium *tert*-butyl oxide catalyst (Scheme 1 A). Desired bi- and mono-fluorenes (that is, $^{R}$**F**2 and $^{R}$**F**1) are readily produced through the methylation of $^{R}$**F**2**H**2/$^{R}$**F** with MeI and potassium *tert*-butyl oxide as base (Scheme 1 A/B). Synthesis of $^{C}$**F**2 was carried out by following the procedure shown in Scheme 1 C. First, the intermediate $^{Br4}$**F**2 was generated by condensation of 2,7-dibromofluorene into $^{Br4}$**F**2**H**2 followed by its methylation. The bromide was then converted to a boron ester using Pd(dppf)$Cl_2$ catalyst, which was reacted with allyl bromide to produce $^{Al4}$**F**2. Intramolecular olefin metathesis reaction allowed us to prepare the $^{C}$**F**2 precursor in good yield, which was then subjected to Pd/C catalyzed hydrogenation, producing $^{C}$**F**2 as a final product. The $^{R}$**F**2 and $^{C}$**F**2 torsionomers and their model compounds $^{R}$**F**1 were fully characterized by $^{1}$H/$^{13}$C NMR spectroscopy (Figure 2 A) and X-ray crystallography (Figure 2 B); see Supporting Information for full details.

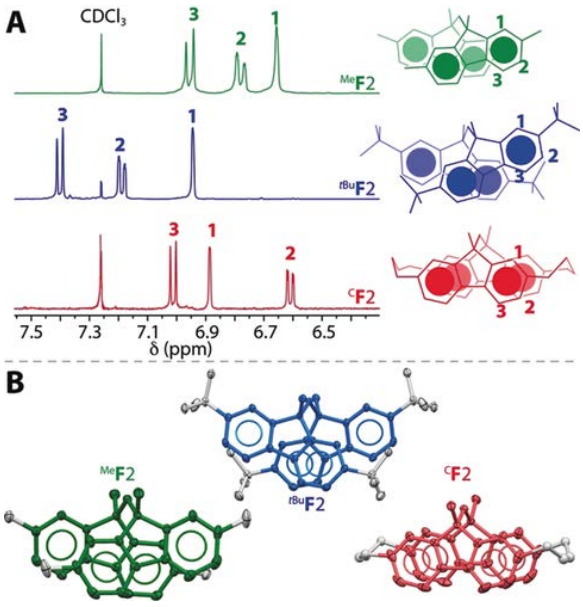


**Figure 2** A) Partial $^{1}$H NMR spectra of $^{Me}$**F**2, $^{tBu}$**F**2, and $^{C}$**F**2 in $CDCl_3$ at 22 °C. B) ORTEP diagrams (50 % diagram) of $^{Me}$**F**2, $^{tBu}$**F**2, and $^{C}$**F**2 highlighting varied cofaciality of the torsionomers.

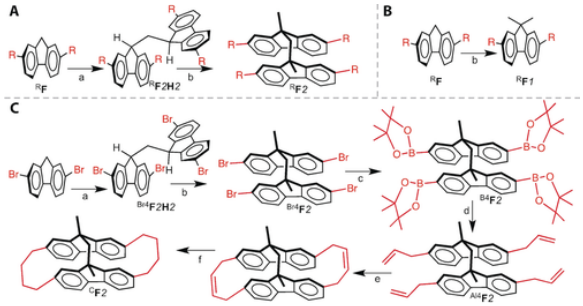


**Scheme 1** a) 10 % mol KO$^{t}$Bu, paraformaldehyde 0.5 equiv, DMF, 20 °C 2 h; b) KO$^{t}$Bu 3 equiv, MeI 3 equiv, THF, 0 °C 12 h; c) $(BPin)_2$ 4.1 equiv, KOAc 4.2 equiv, $Pd(dppf)Cl_2$ 5 % mol, 1,4-dioxane, reflux 12 h; d) Allyl bromide 8 equiv, $Na_2CO_3$ 10 equiv, $Pd(PPh_3)_4$, 1,2-dimethoxyethane, reflux 12 h; e) Grubbs's II 2 % mol, benzene, RT 24 h; f) $H_2$, Pd/C, benzene, 2 h.

The characteristic absorption bands in the electronic spectra of $^{C}$**F**2, $^{Me}$**F**2, and $^{tBu}$**F**2 are comprised of similar vibronic features and the wavelength of the absorption maximum is nearly invariant, that is, $\lambda_{max}$=272±2 nm (Figure 3). In contrast, emission spectra of **F**2 derivatives display a strong dependence on the cofaciality between fluorene moieties (Figure 2). First, the emission spectrum of $^{C}$**F**2 shows a broad excimeric-like band at 402 nm with the lifetime ($\tau$) of 3.8 ns. While the emission spectrum of $^{Me}$**F**2 displays a similar excimeric band at 400 nm ($\tau$=6.5 ns), it also contains a weak band at 325 nm ($\tau$=2.4 ns), which corresponds to the region where emission of $^{Me}$**F**1 monomer occurs (Supporting Information, Figure S3). This indicates that two minima must be present on the potential energy surface (PES) of the $S_1$ excited state of $^{Me}$**F**2. Indeed, TD-DFT calculations at the benchmarked[12, 24, 25] B1LYP40-D3/6-31G(d)+PCM($CH_2Cl_2$) revealed the presence of two equilibrium structures of $^{Me}$**F**2 on the excited state PES, with different exciton delocalization as represented by the transition-density plots in Figure 3. In the global-minimum excimeric sandwich-like structure, the exciton is delocalized over both fluorenes, while in the higher-energy displaced $^{Me}$**F**2, the exciton is localized on a single fluorene.

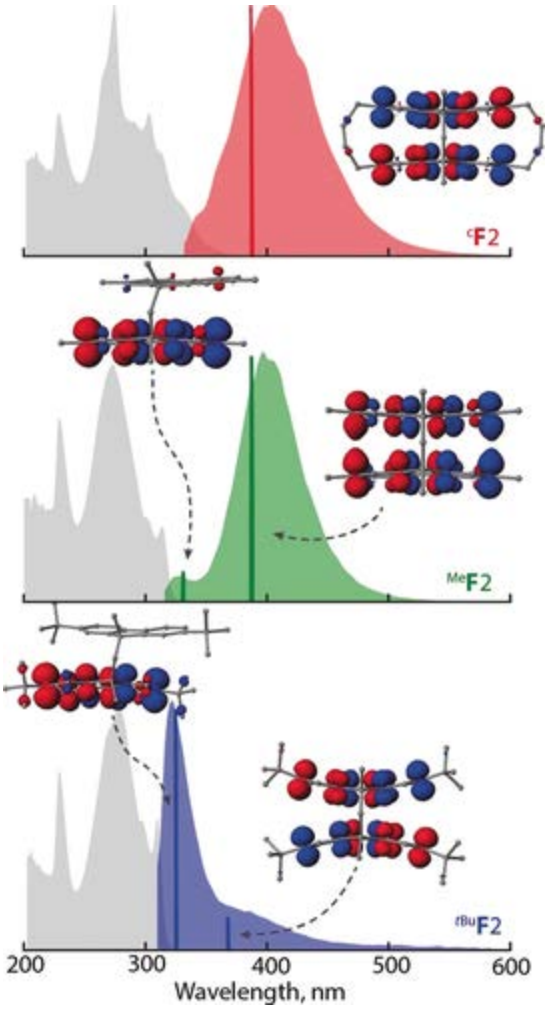


**Figure 3** Absorption (gray) and emission (colored) spectra of $^{C}$**F**2, $^{Me}$**F**2, and $^{tBu}$**F**2 in $CH_2Cl_2$ at 22 °C. Sticks represent the emission wavelength calculated using TD-B1LYP40-D3/6-31G(d)+PCM($CH_2Cl_2$). Transition-density plots are shown for the equilibrium structures of $^{C}$**F**2, $^{Me}$**F**2, and $^{tBu}$**F**2.

In contrast to unhindered $^{Me}$**F**2, the emission spectrum of sterically hindered $^{tBu}$**F**2 displays strong monomeric and weak excimeric bands at 325 and 380 nm, with corresponding lifetimes of 0.4 ns and 1.5 ns, respectively. This suggests that the steric hindrance imposed by the bulky *t*Bu groups must destabilize a sandwich-like conformation in favor of the conformation where two fluorenes are displaced. Indeed, TD-DFT calculations showed the presence of two energetically similar equilibrium structures on the excited state PES of $^{tBu}$**F**2, corresponding to a sandwich-like conformation with exciton delocalized over both fluorenes and a displaced conformation with exciton fully localized on a single fluorene (Figure 3).

Cyclic voltammograms of $^{C}$**F**2, $^{Me}$**F**2, and $^{tBu}$**F**2 show (Figure 4 A) two reversible oxidation waves, with the first oxidation potential ($E_{ox}$) increasing gradually from 0.66 to 0.77 to 0.86 V vs. $Fc/Fc^{+}$, respectively. Comparison with the appropriate model compounds ($^{Me}$**F**1 and $^{tBu}$**F**1) shows that stabilization of the cationic charge, that is, $\Delta E_{ox} = E_{ox}(^{R}\mathbf{F}1) - E_{ox}(^{R}\mathbf{F}2)$, is largest for $^{C}$**F**2 ($\Delta E_{ox}$=360 mV) and decreases as the concomitant energetic penalty of adopting a sandwich-like arrangement increases in $^{Me}$**F**2 ($\Delta E_{ox}$=250

mV) and $^{tBu}$**F**2 ($\Delta E_{ox}$=160 mV). Despite the significant steric hindrance imposed by *t*Bu groups in $^{tBu}$**F**2, the hole stabilization of 160 mV remains significant, highlighting our prior finding that a hole can be stabilized even when there is a minimal orbital overlap.[10, 11]

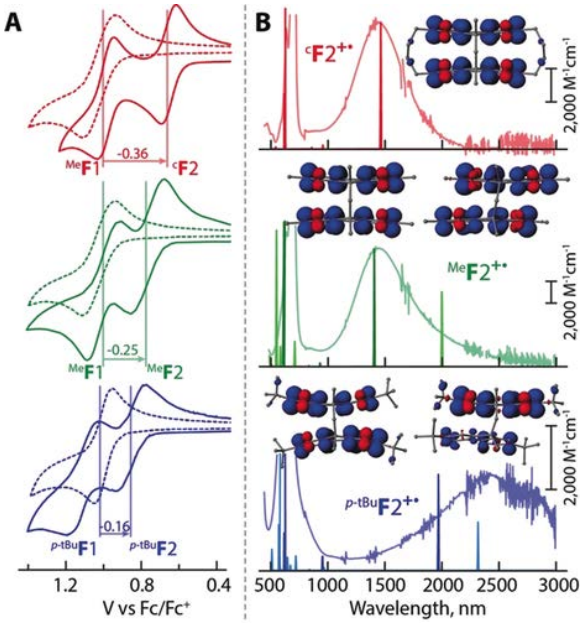


**Figure 4** A) Cyclic voltammograms of 2 mM $^{c}$**F**2, $^{Me}$**F**2, $^{tBu}$**F**2 (solid lines) and their corresponding monomeric model compounds (dashed lines) in $CH_2Cl_2$ (0.1 m *n*-$Bu_4NPF_6$) at a scan rate of 100 mV $s^{-1}$ and 22 °C. B) Electronic absorption spectra of $^{c}$**F**2$^{+\cdot}$, $^{Me}$**F**2$^{+\cdot}$, and $^{tBu}$**F**2$^{+\cdot}$ in $CH_2Cl_2$ at 22 °C. Sticks represent excitation wavelength calculated using TD-B1LYP40-D3/6-31G(d)+PCM($CH_2Cl_2$); dark color corresponds to the sandwich-like structure and light color corresponds to the displaced structure of $^{R}$**F**2.

We generated the cation radicals of $^{Me}$**F**2, $^{tBu}$**F**2, and $^{c}$**F**2 via quantitative[26] redox titrations using robust aromatic oxidants [**THEO**$^{+\cdot}$][$SbCl_6^-$] and **NAP**$^{+\cdot}SbCl_6$ (see details in the Supporting Information).[27] Reproducible spectra of both $^{c}$**F**2$^{+\cdot}$ and $^{Me}$**F**2$^{+\cdot}$ show a nearly identical intense intervalence band centered at 1418 nm (Figure **4** B), signifying that the $^{Me}$**F**2$^{+\cdot}$ structure is identical to that of $^{c}$**F**2$^{+\cdot}$, that is, corresponding to a sandwich-like arrangement of fluorenes, and the cationic charge is delocalized over both fluorenes via strong through-space electronic coupling. Indeed, (TD)-DFT calculations confirmed that the intense near-IR band corresponds to sandwich-like conformations of $^{c}$**F**2$^{+\cdot}$ and $^{Me}$**F**2$^{+\cdot}$, where the charge/spin is delocalized over both fluorenes (Figure **4** B). Our calculations also predict a displaced conformation of $^{Me}$**F**2$^{+\cdot}$ that lies 1.4 kcal $mol^{-1}$ higher in energy than the sandwich-like structure, and also displays spin/charge delocalization over both fluorenes, suggesting that even a minimal through-space orbital overlap is sufficient to promote hole delocalization in bifluorenes. This is in contrast to the excited state of $^{Me}$**F**2, where in the displaced conformation the exciton is localized on a single fluorene (Figure **3**).

The electronic spectrum of $^{tBu}$**F**2$^{+\cdot}$ shows a much less intense intervalence band that is shifted to longer wavelength (2400 nm), suggesting a reduced electronic coupling and/or increased reorganization energy in $^{tBu}$**F**2$^{+\cdot}$ as compared to those in $^{c}$**F**2$^{+\cdot}$ and $^{Me}$**F**2$^{+\cdot}$. DFT calculations showed that two energetically

similar ($\Delta G$=3.5 kcal mol$^{-1}$) conformations of $^{t\mathrm{Bu}}$**F**2$^{+\cdot}$ may exist. The sandwich-like arrangement displays a significant puckering of the fluorene moieties owing to the steric hindrance from bulky *t*Bu groups, yet the spin/charge remains delocalized over both fluorenes. In the displaced $^{t\mathrm{Bu}}$**F**2$^{+\cdot}$, the spin/charge is largely localized on a single fluorene, due to the significant displacement and therefore reduced orbital overlap/electronic coupling.

Additional insights come from gas-phase spectra of the three torsionomers, obtained via laser induced fluorescence (LIF) spectroscopy using a heated supersonic nozzle; details are provided in the Supporting Information. As shown in Figure 5, the differences in these spectra are striking. The spectrum of $^{\mathrm{Me}}$**F**2 (green) is similar to that of **F**2 (black) in displaying a broad and largely unresolved profile; the breadth is explained in the terms of an underlying progression in the torsional motion which is broadened by the fast dynamics and strong modulation of the electronic coupling (Figure 1 A). The underlying progression is clearly seen in the spectrum of $^{t\mathrm{Bu}}$**F**2 (blue), absent any spectral broadening. On the other hand, the spectrum of $^{\mathrm{C}}$**F**2 (red) is both sharp and distinct, and strikingly red-shifted. Here, the torsional libration is quenched and the Franck–Condon active vibration corresponds to a "breathing" type motion of the two subunits (see Figure S14 in Supporting Information). The dramatic consequences of steric hindrance in the $^{t\mathrm{Bu}}$**F**2 derivative can be further seen in a comparison with unsubstituted **F**2 (Figure 5, pale blue vs. black). Here, the underlying torsional progression is clearly evidenced, as the breadth of the spectra is similar. A more detailed analysis of these spectra is beyond the scope of this article and will be reported in future.

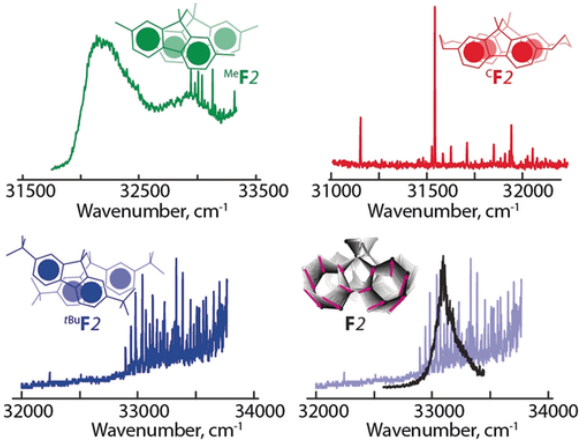


**Figure 5** Laser-induced fluorescence spectra of $^{\mathrm{Me}}$**F**2 (green), $^{t\mathrm{Bu}}$**F**2 (blue), $^{\mathrm{C}}$**F**2 (red), and **F**2 (black) in the gas-phase. Sharp transitions in the spectrum of $^{\mathrm{Me}}$**F**2 reflect monomeric impurity. Comparison of the LIF spectra of **F**2 (black) with $^{t\mathrm{Bu}}$**F**2 (blue) shows the underlying torsional progression.

In conclusion, we have used a set of novel torsionomers to examine the contrasting requirements for exciton and hole stabilization in π-stacked assemblies. Exciton stabilization requires a perfect sandwich-like arrangement, as evidenced by the presence of strong excimeric-like emission only in $^{\mathrm{C}}$**F**2 and $^{\mathrm{Me}}$**F**2. In contrast, cationic charge can be delocalized even for structures where the path to cofaciality is sterically hindered, that is, $^{t\mathrm{Bu}}$**F**2, as judged by the 160 mV hole stabilization and the

presence of a near-IR transition in its cation radical spectrum. These findings underscore important design principles for next generation optoelectronic materials.

## Acknowledgements

We thank the NSF (CHE-1508677) and NIH (R01-HL112639-04) for financial support. The calculations were performed on the high-performance computing cluster Père at Marquette University and XSEDE.

## Conflict of interest

The authors declare no conflict of interest.

References

1 G. I. Livshits, A. Stern, D. Rotem, N. Borovok, G. Eidelshtein, A. Migliore, E. Penzo, S. J. Wind, R. Di Felice, S. S. Skourtis, *Nat. Nanotechnol.* 2014, **9**, 1040.
2 Z. Zheng, N. R. Tummala, Y.-T. Fu, V. Coropceanu, J.-L. Brédas, *ACS Appl. Mater. Interfaces* 2017, **9**, 18095– 18102.
3 C. Kaufmann, W. Kim, A. Nowak-Król, Y. Hong, D. Kim, F. Würthner, *J. Am. Chem. Soc.* 2018, **140**, 4253– 4258.
4 P. Ottiger, H. Köppel, S. Leutwyler, *Chem. Sci.* 2015, **6**, 6059– 6068.
5 M. Miyazaki, M. Fujii, *Phys. Chem. Chem. Phys.* 2015, **17**, 25989– 25997.
6 R. Kusaka, Y. Inokuchi, T. Ebata, *J. Chem. Phys.* 2012, **136**, 044304.
7 P. A. Pieniazek, S. E. Bradforth, A. I. Krylov, *J. Chem. Phys.* 2008, **129**, 074104.
8 E. S. S. Iyer, A. Sadybekov, O. Lioubashevski, A. I. Krylov, S. Ruhman, *J. Phys. Chem. A* 2017, **121**, 1962– 1975.
9 J. Vura-Weis, S. H. Abdelwahed, R. Shukla, R. Rathore, M. A. Ratner, M. R. Wasielewski, *Science* 2010, **328**, 1547– 1550.
10 N. Reilly, M. Ivanov, B. Uhler, M. Talipov, R. Rathore, S. A. Reid, *J. Phys. Chem. Lett.* 2016, **7**, 3042– 3045.
11 B. Uhler, M. V. Ivanov, D. Kokkin, N. Reilly, R. Rathore, S. A. Reid, *J. Phys. Chem. C* 2017, **121**, 15580– 15588.
12 D. Kokkin, M. V. Ivanov, J. Loman, J.-Z. Cai, R. Rathore, S. A. Reid, *J. Phys. Chem. Lett.* 2018, **9**, 2058– 2061.
13 K. Kawai, T. Kimura, H. Yoshida, A. Sugimoto, S. Tojo, M. Fujitsuka, T. Majima, *Bull. Chem. Soc. Jpn.* 2006, **79**, 312– 316.
14 S. Samori, M. Fujitsuka, T. Majima, *Res. Chem. Intermed.* 2013, **39**, 449– 461.
15 Y. Gao, H. Liu, S. Zhang, Y. Shen, Y. Ge, B. Yang, *Phys. Chem. Chem. Phys.* 2018, **20**, 12129– 12137.
16 O. P. Dimitriev, Y. P. Piryatinski, Y. L. Slominskii, *J. Phys. Chem. Lett.* 2018, **9**, 2138– 2143.
17 B. L. Cannon, D. L. Kellis, L. K. Patten, P. H. Davis, J. Lee, E. Graugnard, B. Yurke, W. B. Knowlton, *J. Phys. Chem. A* 2017, **121**, 6905– 6916.
18 J. K. Kochi, R. Rathore, P. L. Magueres, *J. Org. Chem.* 2000, **65**, 6826– 6836.
19 M. V. Ivanov, N. J. Reilly, B. Uhler, D. Kokkin, R. Rathore, S. A. Reid, *J. Phys. Chem. Lett.* 2017, **8**, 5272– 5276.
20 R. Rathore, S. H. Abdelwahed, I. A. Guzei, *J. Am. Chem. Soc.* 2003, **125**, 8712– 8713.
21 M. R. Talipov, M. V. Ivanov, S. A. Reid, R. Rathore, *J. Phys. Chem. Lett.* 2016, **7**, 2915– 2920.
22 M. W. Haenel, H. Irngartinger, C. Krieger, *Chem. Ber.* 1985, **118**, 144– 162.
23 J. Wang, W. Wan, H. Jiang, Y. Gao, X. Jiang, H. Lin, W. Zhao, J. Hao, *Org. Lett.* 2010, **12**, 3874– 3877.
24 M. R. Talipov, A. Boddeda, Q. K. Timerghazin, R. Rathore, *J. Phys. Chem. C* 2014, **118**, 21400– 21408.
25 M. Ivanov, M. Talipov, T. Navale, R. Rathore, *J. Phys. Chem. C* 2018, **122**, 2539– 2545.
26 M. R. Talipov, A. Boddeda, M. M. Hossain, R. Rathore, *J. Phys. Org. Chem.* 2016, **29**, 227– 233.
27 "Robust Aromatic Cation Radicals as Redox Tunable Oxidants": M. R. Talipov, R. Rathore in *Organic Redox Systems: Synthesis Properties, and Applications*, Wiley, Hoboken, 2015, p. 131.